



Research Article

Designing of system for high grade heat recovery in thermal cooling system for process heat applications

Alka SOLANKI^{1,*}, Yash PAL¹

¹National Institute of Technology, Kurukshetra Haryana, 136119, India

ARTICLE INFO

Article history

Received: 29 October 2020

Revised: 08 February 2021

Accepted: 11 February 2021

Keywords:

Single Effect Absorption System; Water-Lithium Bromide; Process Heat; Dairy Industry

ABSTRACT

An experimental investigation on design of a vapour absorption system using LiBr-H₂O for high grade heat recovery in thermal cooling system for process heat applications has been conducted. A 1.5 kW cooling capacity of the LiBr-H₂O vapour absorption system has been designed and tested under various operating conditions. Generator temperature, absorber temperature, condenser temperature and evaporator temperature have been varied and performance of LiBr-H₂O vapour absorption system has been analysed. Experimental results are presented in terms of COP and circulation ratio. Further, to validate the results thermodynamic model is developed using first law of thermodynamics and simulate in Engineering Equation Solver. The COP and the circulation ratio estimated through simulations and experiments have been in good agreement with $\pm 5\%$ standard deviation. Further, this research work is beneficial for dairy industries in process heat applications and realizing the importance of the need for energy conservation in dairy industries.

Cite this article as: Solanki A, Pal Y. Designing of system for high grade heat recovery in thermal cooling system for process heat applications. J Ther Eng 2023;9(3):679–701.

INTRODUCTION

The dairy industry has been growing at a good pace worldwide. The demand for dairy products has been increasing steadily with the improvement in living standards of people all around [1]. The energy in the processing of dairy products in any dairy industry plays a significant role. Most of the dairy industries of developing countries mainly rely on low-grade energy sources such as wood, kerosene oil and diesel etc. for steam generation and other applications. The rest of the dairy sectors rely on high-grade energy, i.e. electricity. The dairy industry use adequate

quantity of power in process heat applications [2] which shows a strong evidence of increase in level of CO₂ emission [3]. The continuous usage of fossil fuels outcomes in ozone depletion and global warming [4]. Thus, there is a great need to improve the efficiency of dairy industries and reducing the level of CO₂ emission for contributing to sustainable development. Hence, there is a need for the selection of a new renewable energy technologies [5].

Tremendous growth has been observed in the renewable energy sector worldwide. Solar energy is the most popular choice for absorption cooling system [6]. Several innovative and efficient technologies are available that can be used for

*Corresponding author.

*E-mail address: alkasolanki10@gmail.com

This paper was recommended for publication in revised form by Regional Editor Ahmet Selim Dalkılıç



process heat applications in dairy industries. In particular, renewable energy can aid in cost-cutting in plus to reducing carbon footprints. Further, dairy industries are acquiring green energy technologies to meet their needs. For instance, Mahanand Dairy situated in Latur, India has been using huge solar dish collector to meet their thermal needs [7].

The global dairy industry is sincerely exploring renewable energy for dairy processing plants of the future as it improves efficiency, reduces cost and complies with environmental responsibilities [8]. The Integration of a vapor absorption system in process heat applications in the dairy industry can provide energy-efficient opportunities. Using such technology towards savings in electricity can replace the existing system in process heat applications. The collective savings of energy in the chilling process and hot water generation can have a significant effect on whole dairy power charges. Zhang et al. [9] analyzed electricity usage and production cost of milk in eleven dairy farms in China and evaluated the potential of solar energy generated by PV water pumping system. Desai et al. [1] discussed the implementation of solar energy for reliable dairy advancement. Panchal et al. [10] discussed the various research works on milk pasteurization using solar energy, which is the right solution in terms of energy-saving and efficiency. Yildirim et al. [11] analyzed thermodynamically the milk pasteurization system that is assisted by geothermal energy. The results indicated the increase in pasteurization capacity with the raise in geothermal resource flow rate. Cocco et al. [12] manifested the use of solar technology as an excellent option if both the power and heat are required at a common point of application. Further, solar technology has flexibility features like using different control variables; the local electricity demand may also be fulfilled. Praveen et al. [13] studied the classification, working principle, applications, benefits and limitations of solar thermal power in the milk and their product industry. Sandeet al. [14] concluded that the solar energy could be used in the dairy industry for solar drying, for pumping dairy fluid, for room conditioning, for cold storage of milk & milk products, for lighting and electric fencing. Anderson et al. [15] simulated the performance of four types of solar representative concerning their adaptability for heating and cooling in the milk and other industry. Finally, it is concluded that both flat plate and evacuated tube-based solar collector systems have better performance and make it sincere contribution to energy saving in the dairy industry. Modi et al. [16] utilized the waste heat in milk process plants that resulted in low investment with high energy saving. Ketfi et al. [17] had done a simulation study on the single-effect absorption system by varying evaporator, condenser, absorber and generator temperature. Manu et al. [18] conducted a simulation research of a sole-phase absorption heat pump mechanism for chip cooling using Matlab (2008b). Lamineet al. [19] studied an absorption refrigeration mechanism functioning in the industrial manufacturing of detergent (Henkel Algeria). Pandya et al. [20] had done a simulation study of

1 TR capacity using EES software. The result revealed that the temperature of generator decline with rise in evaporator temperature and further raises with the temperature of condenser. Patel et al. [21] investigated a LiBr-H₂O vapour-absorption mechanism designed for the cooling capacity of 140 kW. The various parameters viz. heat load, circulation ratio, pump work, COP, COP_{rev} and η_{ex} are analyzed at different operating conditions. The results have shown a rise in the heat load on the generator and absorber increases with the the exit temperatures of generator and condenser. Uckan and Yousif [22] simulated the single effect vapour absorption system under the climate of Duhok City situated in the North of Iraq via utilizing TRNSYS 17 programs and the COP of the mechanism was found as 0.63. Iyer and Mastorakis [23] discussed the energy conservation measures in dairy industries. Further, this study provides the energy conservation techniques for dairy industries. Singh et al. [24] stated that requirements of energy and temperature range in milk processing plants are amenable for the adoption of solar energy.

Zhu and Gu [25] analyzed the performance of a novel absorption system for cooling and heating applications. The active component of the sorbent used in this study is sodium thiocyanate (NaSCN). Ammonia (NH₃) is chosen as sorptive. The results show that the COP of cooling and heating increases with the heat source temperature and decreases with the cooling water inlet temperature, but the system exergetic efficiency does not show the same trends for both cooling and heating applications. Farshi et al. [26] presented systematic procedure for estimating thermodynamic properties of working fluids (Ammonia/LiNO₃ and Ammonia/NaSCN) formulated. Mathematical expressions also formulated for estimating thermodynamic properties (Specific enthalpy & Specific entropy) of Ammonia/LiNO₃ and Ammonia/NaSCN. Singh and verma [27] exploited artificial intelligence for performing energy analysis of absorption refrigeration system (ARS) with water-lithium chloride as working fluid. The maximum difference between the predicted results and experimental data of thermodynamic properties are less than 1%. Value of the coefficient of multiple determinations is 1 for test data set and can be considered satisfactorily for using ANN in vapour absorption refrigeration system. Singh and verma [28] have done a simulation for estimating thermodynamic properties (specific enthalpy and specific entropy) of water-lithium bromide solution using artificial neural network under MATLAB Simulink environment. AI-Simulink simulator is developed by deploying extracted weights and bias from modeled artificial neural networks. Optimized performance is achieved with 2-10-2 ANN architecture which is validated on the basis of mean square error, coefficient of multiple determination (R²), and absolute relative error. Oudina [29] investigation of natural convection heat transfer stability in cylindrical annular with discrete isoflux heat source of different lengths. The results show that the increase of heat source length ratio decreases the critical Rayleigh number.

Previous literature have done simulation as well as experimental results on vapour absorption system or change the working fluids but present research is focused on utilizing of vapour absorption system in process heat application in dairy industry. However, a minimal study on the application of an absorption system in process heat applications in the dairy industry has been observed. Accordingly, in the current work, an experimental study on the feasibility of vapor absorption system in process heat applications in the dairy industry has been carried out. An absorption system has been designed at National Institute of Solar Energy (NISE), Gurugram, India. The experiments have been conducted on the experimental set-up using LiBr-H₂O. Further, a mathematical model has been developed using Engineering Equation Solver (EES) Academic Professional Version: V10.644 [2019-06-10] software to validate the experimental results. The influence of generator, absorber, condenser and evaporator temperature on coefficient of performance and circulation ratio have been investigated. Finally, the feasibility of a single-effect vapor absorption system in process heat applications in the dairy industry has been discussed.

Thermodynamic Modelling

The first law of thermodynamics has been used to perform the analysis. Conservation of mass and energy balance has been applied to each component of the absorption system. In this way, steady-state equations have been formulated.

System Description

A model of single-effect vapor absorption system has been developed, as shown in Figure 1. The system consists of an absorber, a generator, a condenser, an evaporator, a solution heat exchanger (SHE), a refrigerant heat exchanger (RHE), a solution expansion valve, a pump and a refrigerant expansion valve.

The cycle has two circuits: the refrigerant circuit (7-11) and LiBr-H₂O solution circuit (1-6). Heat is supplied to the generator (Q_g) which evaporates the refrigerant H₂O at high pressure (P_c), the evaporated H₂O is then convected to the condenser (7). The condenser dissipates heat (Q_c) and then H₂O changes phase from vapour to liquid (8).

Then, the refrigerant H₂O is flowed to refrigerant expansion valve (RTV) via refrigerant heat exchanger to reach evaporation pressure (P_e); consequently, it led to the

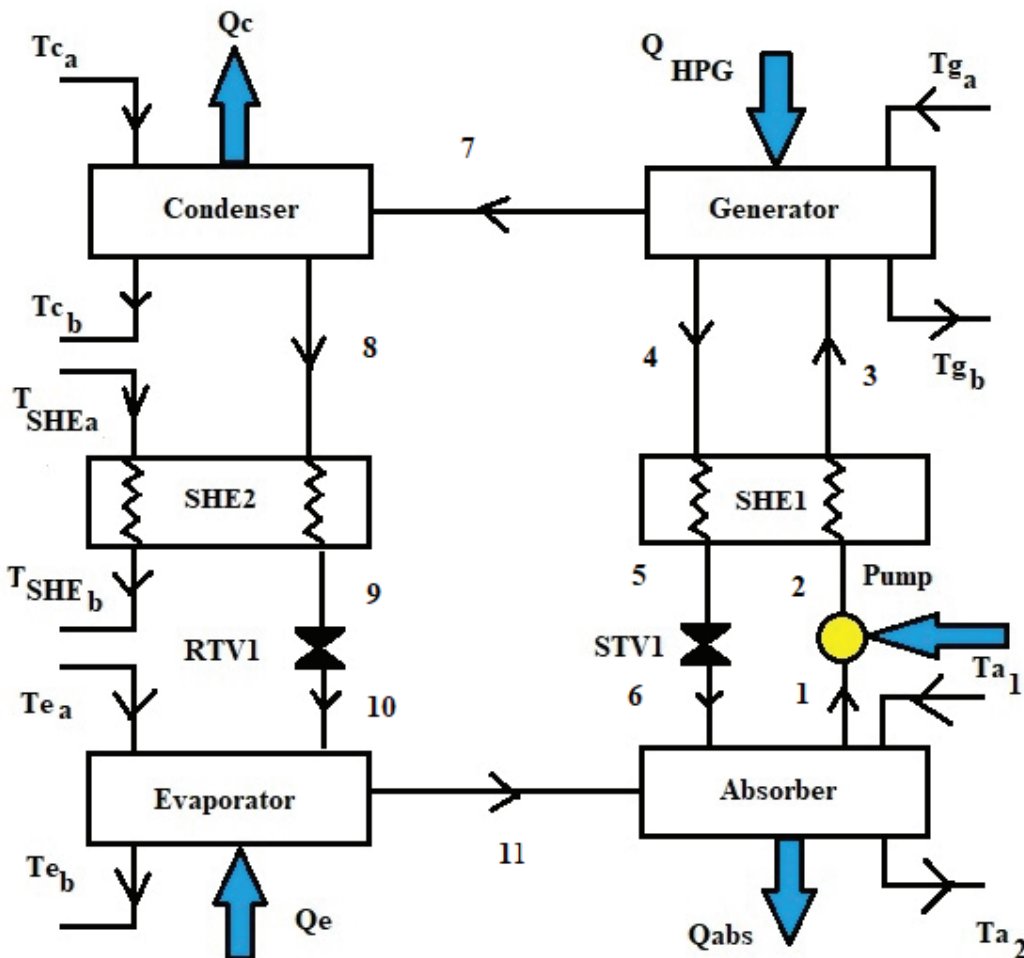


Figure 1. Model of the sole-impact vapor absorption mechanism.

evaporator (10). The cooling process is conducted in the evaporator once the refrigerant soak up heat (Q_c) from the environment, this causes that refrigerant evaporates once again (11) and then led to the absorber, where it mixes with the weak solution coming from the generator. Once they mix-up, a LiBr–H₂O solution with low concentration is formed and release heat (Q_a). After that, the solution is pumped to the generator (3) until it reaches condenser pressure (P_c) via a solution heat exchanger which increases solution temperature.

The cycle initiates after getting sufficient temperature in the generator. Apart of the refrigerant evaporates and goes to the condenser (7). The rest of the solution with high concentration is led to the heat exchanger (4) where its temperature is lowered. Then it is passed by a throttle valve (TV) where its pressure is decreased to the evaporation pressure (P_e). Finally, it comes to the absorber, and the cycle continues. Further, the following assumptions were made for thermodynamic modelling.

- i. The analysis has been done for steady flow conditions.
- ii. The refrigerant at the exit of condenser has been assumed to be a saturated liquid.
- iii. The refrigerant at the exit of the evaporator has been assumed to be saturated vapour.
- iv. A strong solution has been assumed to leave of the absorber at absorber temperature.
- v. The isenthalpic process of throttling in the expansion valve and solution valve has been assumed.
- vi. No heat exchange between the system and surroundings has been assumed.
- vii. The refrigerant vapour leaving the generator has been assumed to be superheated.
- viii. Heat exchanger effectiveness (ϵ_{SHE1} , ϵ_{SHE2} and ϵ_{SHE3}) has been taken as 0.7.

Mass conservation

It involves a mass equilibrium of total mass and every material of the solution. For steady state-flow, the governing equations of mass and type of material conservations are:

$$\sum m_i - \sum m_o = 0 \quad [30] \quad (1)$$

$$\sum m_i X_i - \sum m_o X_o = 0 \quad (2)$$

where, m is the mass flow rate and X is the mass fraction of LiBr in the solution.

Using Eq. (1) and (2), the mass balancing of each components of the absorption system has been formulated as:

Generator:

$$m_3 = m_4 + m_7 \quad (3)$$

$$m_3 X_3 = m_4 X_3 + m_7 X_3 \quad (4)$$

Condenser:

$$m_7 = m_8 \quad (5)$$

RHE:

$$m_8 = m_9 \quad (6)$$

RTV:

$$m_9 = m_{10} \quad (7)$$

Evaporator:

$$m_{10} = m_{11} \quad (8)$$

Absorber:

$$m_1 = m_{11} + m_6 \quad (9)$$

Pump:

$$m_1 = m_2 \quad (10)$$

SHE:

$$m_2 = m_3 \quad (11)$$

$$m_4 = m_5 \quad (12)$$

STV:

$$m_5 = m_6 \quad (13)$$

Where suffix, $i = 1, 2, \dots, 11$ shows mass flow rate at different state points

2.3 First law analysis

The first law of thermodynamics for each component of the absorption system is expressed as follows:

$$\sum \dot{Q} - \sum \dot{W} = \sum m_o h_o - \sum m_i h_i \quad [30] \quad (14)$$

Energy balance equations of each component of the absorption system are as:

Condenser:

$$Q_c = m_7(h_7 - h_8) = m_c(h_{cb} - h_{ca}) \quad (15)$$

RHE:

$$Q_{RHE} = m_8(h_8 - h_9) = m_{RHE}(h_{RHEb} - h_{RHEa}) \quad (16)$$

Evaporator:

$$Q_e = m_{11}(h_{11} - h_{10}) = m_e(h_{ea} - h_{eb}) \quad (17)$$

Absorber:

$$Q_a = m_{11}h_{11} + m_6h_6 - m_1h_1 = m_a(h_{a2} - h_{a1}) \quad (18)$$

Pump:

$$w_p = m_1 v_1 (P_2 - P_1) / 1000 \quad (19)$$

SHE:

$$Q_{SHE} = m_3(h_3 - h_2) = m_5(h_4 - h_5) \quad (20)$$

Generator:

$$Q_g = m_3h_3 + m_7h_7 - m_4h_4 = m_g(h_{g2} - h_{g1}) \quad (21)$$

The overall performance of the absorption system has been determined by evaluating its coefficient of performance (COP) as:

$$COP = \frac{Q_e}{Q_{HTG} + W_p} \quad [30] \quad (22)$$

where, Q_c is the refrigerant effect, Q_{HTG} is the heat rate in the generator, and W_p is the pump work.

Model validation

The EES code validation has been carried out through comparing the current simulation results with that of Ketfi et al. [12], Kaushik et al. [18] and Modi et al. [31]. A comparison of simulation results has been shown in Table 1. The deviation in COP is -2.83% when compared with Ketfi et al. [12]. Similarly, the deviation in COP is +6.63% and +6.71% of present simulation results when compared with the results of Modi et al. [31] and Kaushik et al. [32],

respectively. The variation in results is due to irreversibility distribution among every component of the absorption system. Also, the current single-impact vapor absorption system is satisfactory for the simulation.

Experimental Test Facility

Experimental set-up with cooling capacity of 1.5 kW has been developed for the feasibility assessment of its applicability in the dairy industry. The test facility has been shown schematically and photographically as Figure 2 and 3, respectively.

Table 1. Comparison of simulation results with the published results

Sr. No.	Published literature	Tg (°C)	Tc (°C)	Ta (°C)	Te (°C)	COP	COP Estimated through the present model using EES	Deviation
1	Ketfi et al. [12]	90	40	40	7	0.775	0.753	-2.83%
2	Modi et al. [17]	87.8	37.8	37.8	7.2	0.7615	0.812	6.63%
3	Kaushik et al. [18]	87.8	37.8	37.8	7.2	0.7609	0.812	6.71%

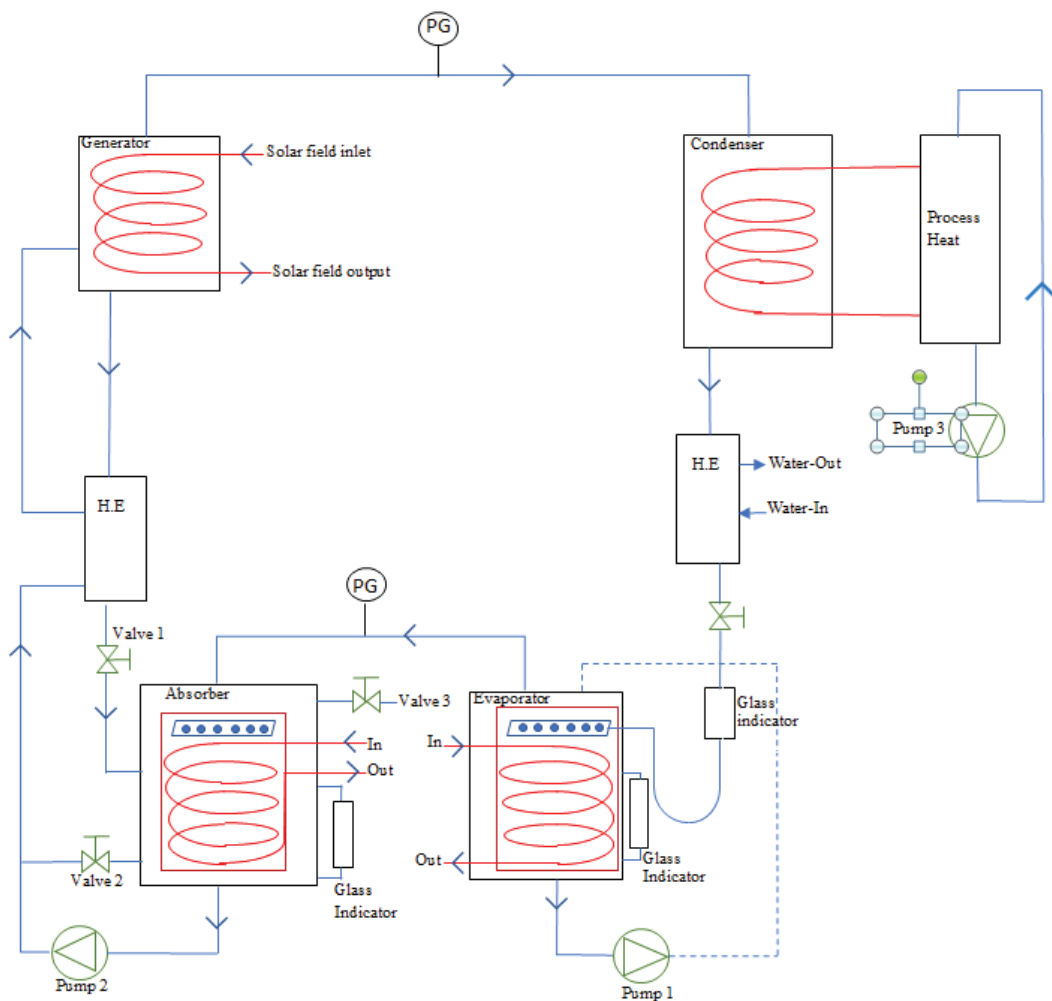


Figure 2. Representative diagram of the practical test facility.



Figure 3. Practical test facility of the vapor absorption system.

All the four seamless vessels used as evaporator, condenser, generator and absorber have been made of copper. In the generator, baffle plates have been provided at the upper end to get pool boiling and to avoid liquid solution droplets going out with water vapours. The evaporator has been designed like a spray column to ensure maximum heat transfer in the present case.

The absorber used in the experimental facility acts as a falling film column. The solution has been made to spray over a cooling coil in the absorber to form a liquid film over the coil to get maximum heat transfer in the present case. The solution heated up with the help of ETC in the generator and the cold solution from the absorber has been made to flow in counter current directions via the annular duct and the inner tube, respectively.

A bypass flow control valve has been employed at the inlet of the heat exchanger to measure the heat exchanger effectiveness. Voltage and current transducers have been used for measuring supply power. The cooling water flow rates across the condenser and the absorber have been

controlled with the help of solenoid control valves. All of the vessels used as the main components of vapour absorption system were provided with sight-glasses to observe liquid levels. Infra-red switches have been employed on the sight glasses to measure the fluid levels. In the steady-state condition, the liquid volume has been measured using sight-glass over a finite time interval. A rotameter has been utilized to measure the flow rate of solution flowing through the absorber.

The performance of the practical mechanism has been analyzed using experimental observations taken above a linear-state processing time of 60 minutes. The experimental outcomes have been recorded by varying the temperatures of the absorber, generator, condenser and evaporator. Further, the details of the measuring instruments have been given in Table 2.

The heat required to regenerate the solution has been produced using an evacuated tube collector, as shown in Figure 4. The internal coils used in the various sub-systems of the experimental facility have been shown

Table 2. The details of the measuring instruments

Sr. No	Measuring Instruments	Range	Resolutions	Parameters
1	Hydrometer	0.990-1.170	0.01	Specific gravity
2	LiDS temperature	J-Type thermocouple	0-600°C	LiDS temperature
3	Flow meter	1 -10 lpm	1 lpm	Flow rate

photographically as Figure 5. The detailed specifications of the collector have been given in Table 3.

Experimental Procedure

Initially, the experimental unit was evacuated using a vacuum pump to remove the condensable gases from the system. The deionized water was used to charge the receiver tank and the evaporator, while the absorber and the generator were arranged with lithium–bromide solution (55% v/v). The thermal input was given to the generator through the evacuated tube collector, and consequently, the solution in the generator vessel started to gain the temperature and pressure. The temperature in the generator was raised to 140°C using the ETC collector and a storage tank.

The pressure was measured using pressure gauges, as shown in the photographic view of the system. Subsequently, the water got evaporated as vapours from the LiBr–H₂O

solution and moved from the generator to the condenser. The vapours at huge temperature and pressure entered into the condenser. The condenser has been designed specially to extract waste heat recovery. The main aim was to extract heat for its conversion into a useful form. The condenser has been employed with helical coils to get maximum heat transfer as shown in Figure 5. The vapours got condensed in the condenser by virtue of the temperature gradient due to circulation cold water at ambient conditions through the helical coils.

The condensed water was collected at the bottom of the condenser tank. The condensed was made to flow through an expansion valve and a heat exchanger. Further the low temperature condensed water entered into the evaporator through a helical coil. The flow of the condensed water was controlled by a valve employed just after a heat



Figure 4. A photographic view of the Evacuated Tube Collector used in the experiments.

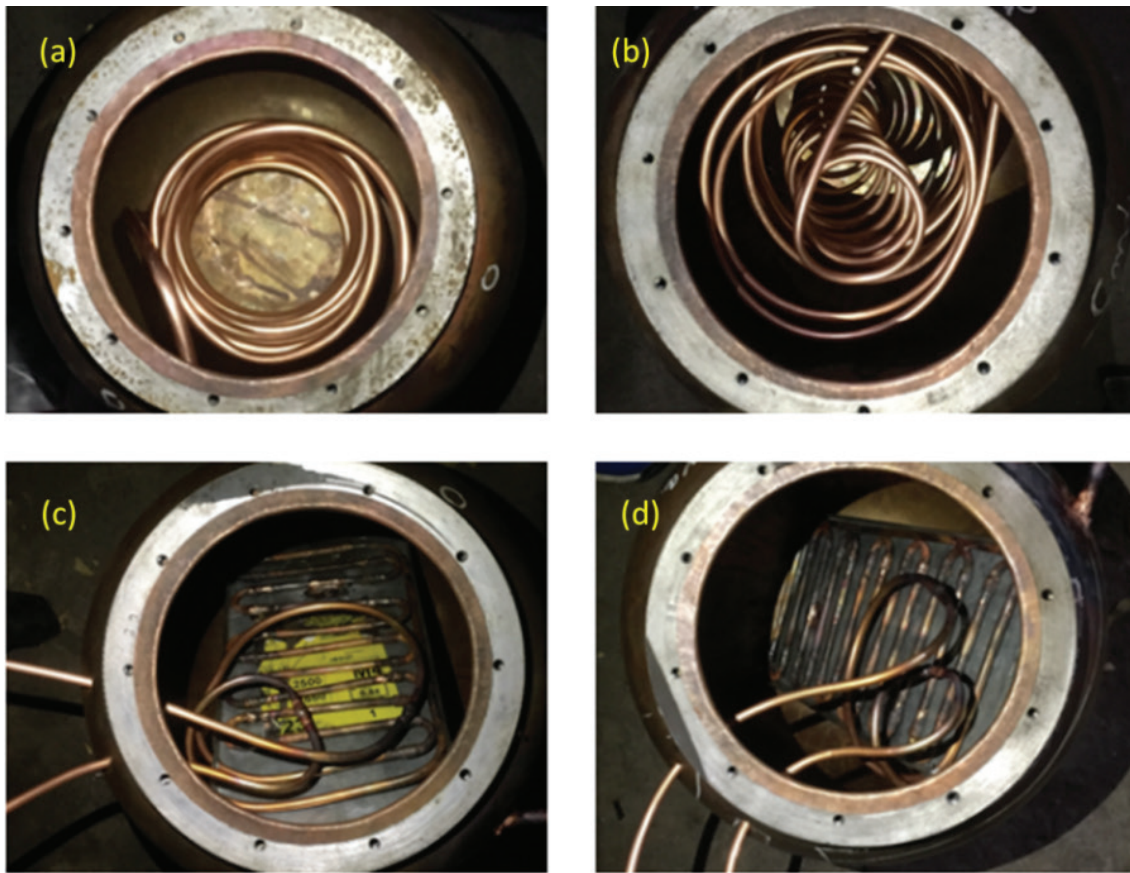


Figure 5. Photographic views of internal coils used in (a) generator, (b) condenser, (c) evaporator and (d) absorber.

Table 3. The detailed specifications of the ETC collector

Material of Glass	Borosilicate Glass
Thickness of Glass Tube	Outer tube thickness: 1.8 mm, inner tube thickness: 1.6 mm
Inner diameter	47 mm
Outer diameter	58 mm
Coefficient of Thermal Expansion	$3.3 \times 10^{-6}/K$
Vacuum rate	$P \leq 5.0 \times 10^{-4} Pa$
Recommended operating pressure	0.2 kg/cm^2
Stagnation Parameter	$Y \geq 290 \text{ M}^2 \text{ }^\circ\text{C/kW}$
Selective coating type	AIN/AIN-SS/CU – Sputtering
Value of absorptance and emittance of the black coating	Absorptance: $\alpha \geq 93.5\%$, Emission rate: $\epsilon \leq 5\%$

exchanger. The heat exchangers having counterflow current were used between the condenser and the evaporator & between the generator and the absorber, respectively to utilize the waste heat throughout the cycle.

Uncertainty Analyses

Generally, the accuracy of the experimental results hinges on the accuracy of the individual measuring

instruments and techniques. The uncertainty of the parameters was calculated based upon the root sum square combination of the effects of each of the individual inputs as presented by Kline and McClintock [33]. For all experimental runs, the maximum uncertainties in the main parameters are shown in Table 4. For the estimated uncertainties in the other variables and parameters used in the current research, additional information is given in Appendix A.

Table 4. Uncertainty analysis

Sr. No	Measuring Instruments	Range	Uncertainty
1	Hydrometer	0.990-1.170	± 0.005
2	LiDS temperature	J-Type thermocouple	± 1.8°C
3	Flow meter	1 -10 lpm	± 0.45lpm

The association for uncertainty examination has been described below:

$$\Delta x = \left[\left(\frac{\partial m}{\partial z_1} \right)^2 (\Delta z_1)^2 + \left(\frac{\partial m}{\partial z_2} \right)^2 (\Delta z_2)^2 + \dots + \left(\frac{\partial m}{\partial z_n} \right)^2 (\Delta z_n)^2 \right]^{\frac{1}{2}} \quad (23)$$

Where x is the reliant variable and Δx is its total uncertainty and m is a function of the independent variable z_1 , Δz_1 is the absolute uncertainty. The relative uncertainty is given by:

$$\frac{\Delta x}{x} = \left[\left(\frac{\partial m}{\partial z_1} \right)^2 \left(\frac{\Delta z_1}{y} \right)^2 + \left(\frac{\partial m}{\partial z_2} \right)^2 \left(\frac{\Delta z_2}{y} \right)^2 + \dots + \left(\frac{\partial m}{\partial z_n} \right)^2 \left(\frac{\Delta z_n}{y} \right)^2 \right]^{\frac{1}{2}} \quad (24)$$

Based on the above interactions, a comprehensive error calculation has been made through uncertainty analysis. The mean of the error and standard deviation for all the observations used to calculate the COP of the system are 0.03 and 13.44 respectively.

RESULTS AND DISCUSSION

An Engineering Equation Solver software is utilized to simulate the vapour absorption system to validate the experimental results and found in good agreement with each other. The experimental set-up was examined with a broad variation of regulating temperatures. The operating parameters for present experimental and simulation work are presented in Table 5. The Comparison of the experimental and simulation results has been carried out by varying the influence of generator, condenser, evaporator and

absorber temperatures on COP and circulation ratio have been discussed in subsequent sub-section 4.1, 4.2, 4.3 and 4.4, respectively.

Impact of generator temperature

The LiBr-Water system has been analyzed by conduction experiments and simulation by varying temperature of the generator, absorber (Q_a), condenser (Q_c), and evaporator (Q_e). The effects of high generator temperature (T_g) on heat flow rates in the generator (Q_g), absorber (Q_a), condenser (Q_c), and evaporator (Q_e) have been shown in Table 6 and Figure 7.

Table 6 shows the experimental and simulation results of effect of generator temperature (T_g) on heat flow rate in generator, absorber, condenser and evaporator at $T_c = 50^\circ\text{C}$, $T_a = 40^\circ\text{C}$, $T_c = 5^\circ\text{C}$, and $e_{HX} = 0.7$. Figure 6 depicts that with an increase of generator temperature heat transfer in

Table 5. Input parameters for simulation

Sr.No.	Input parameters	Values
1	Generator temperature	110°C
2	Condenser temperature	50°C
3	Absorber temperature	40°C
4	Evaporator temperature,	5°C
5	mass flow rate of refrigerant	1 kg/s
6	Heat exchanger effectiveness	0.7

Table 6. Computed heat flow rate in generator, absorber, condenser and evaporator at different generator temperature at ($T_c = 50^\circ\text{C}$, $T_a = 40^\circ\text{C}$, $T_c = 5^\circ\text{C}$, $e_{HX} = 0.7$)

Generator temperature, T_g (°C)	95	100	105	110	115	120	125	130	135	140
<i>Experimental data</i>										
Q_a (kW)	2771	2786	2798	2805	2809	2810	2807	2803	2795	2784
Q_c (kW)	2345	2353	2363	2371	2381	2390	2399	2408	2417	2426
Q_e (kW)	2195	2195	2195	2195	2195	2195	2195	2195	2195	2195
Q_g (kW)	6274	3861	3274	3012	2866	2777	2721	2684	2662	2650
<i>Simulation data</i>										
Q_a (kW)	2917	2933	2945	2953	2957	2958	2955	2950	2942	2931
Q_c (kW)	2468	2477	2487	2496	2506	2516	2525	2535	2544	2554
Q_e (kW)	2311	2311	2311	2311	2311	2311	2311	2311	2311	2311
Q_g (kW)	6604	4064	3446	3170	3017	2923	2864	2825	2802	2789

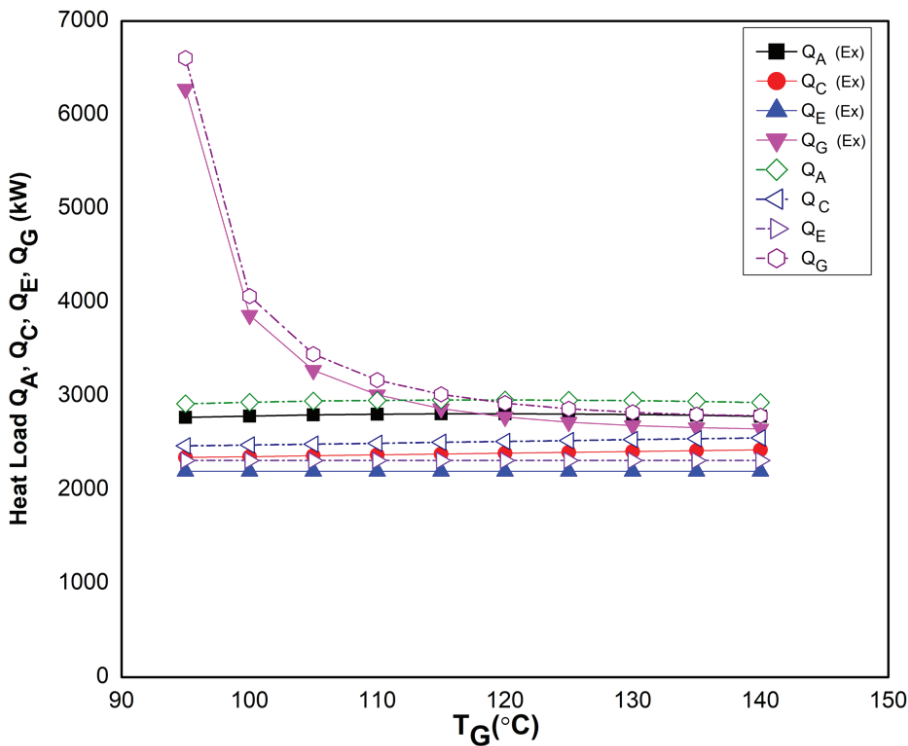


Figure 6. Effect of generator temperature on heat flow rate in generators, absorber, condenser and evaporator ($T_c = 50^\circ\text{C}$, $T_a = 40^\circ\text{C}$, $T_e = 5^\circ\text{C}$, $e_{HX} = 0.7$).

absorber and condenser increases but heat transfer in generator decreases gradually. Moreover, the effect of increase in the generator temperature on heat transfer in evaporator remains constant. It is because with increase in generator temperatures causes circulation ratio to decrease and consequently produce the same effect as mentioned above. Further, experimental and simulation results are in good agreement.

Table 7 shows the experimental and simulation results on effect of generator temperature and on circulation ratio at $T_c = 5^\circ\text{C}$ and $e_{HX} = 0.7$). Figure 7 presents the variation of circulation ratio with generator temperature at different absorber and condenser temperatures. Figure 6 demonstrates that with a raise in generator temperature, circulation ratio decreases with varying absorber temperature. The lowest value of circulation is achieved at low values

Table 7. Computed circulation ratio at different generator temperature ($T_c = 5^\circ\text{C}$, $e_{HX} = 0.7$)

Generator temperature, T_g ($^\circ\text{C}$)	95	100	105	110	115	120	125	130	135	140
<i>Experimental data</i>										
Circulation ratio (CR)										
$T_a = T_c = 20$	1.54	1.43	1.34	1.26	1.18	1.11	1.05	0.99	0.94	0.89
$T_a = T_c = 30^\circ\text{C}$	3.02	2.71	2.45	2.25	2.08	1.93	1.81	1.70	1.60	1.52
$T_a = T_c = 40^\circ\text{C}$	8.76	6.68	5.43	4.61	4.02	3.57	3.22	2.95	2.72	2.52
<i>Simulation data</i>										
Circulation ratio (CR)										
$T_a = T_c = 20^\circ\text{C}$	1.62	1.51	1.41	1.32	1.25	1.17	1.11	1.05	0.99	0.93
$T_a = T_c = 30^\circ\text{C}$	3.18	2.85	2.58	2.37	2.19	2.03	1.90	1.79	1.69	1.60
$T_a = T_c = 40^\circ\text{C}$	9.22	7.03	5.72	4.85	4.23	3.76	3.39	3.10	2.86	2.66

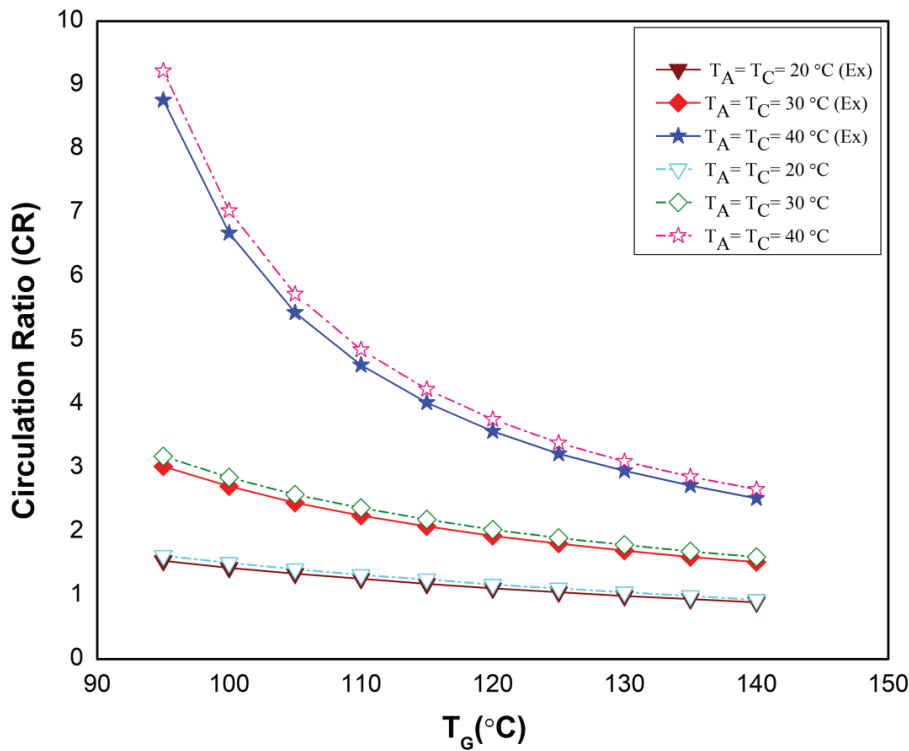


Figure 7. Effect of generator temperature on circulation ratio ($T_c = 5^\circ\text{C}$, $e_{\text{HX}} = 0.7$).

of absorber and condenser temperatures. Similarly, highest value of circulation is attained at low temperatures of absorber and condenser. It is due to fact that with increase in generator temperature, the flow rate of strong solution decreases. Further, experimental and simulation results are in good agreement.

Table 8 shows the experimental and simulation results on coefficient of performance at different generator temperature with $T_c = 50^\circ\text{C}$, $T_e = 5^\circ\text{C}$, and $e_{\text{HX}} = 0.7$. Figure 8 depicts that when the condenser and evaporator temperature is maintained at 50°C , and 5°C with heat exchanger effectiveness of 70%, COP of absorption system increases with the rise in generator temperature. Further, maximum

Table 8. Computed Coefficient of performance at different generator temperature ($T_c = 50^\circ\text{C}$, $T_e = 5^\circ\text{C}$, $e_{\text{HX}} = 0.7$)

Generator temperature, T_g ($^\circ\text{C}$)	95	100	105	110	115	120	125	130	135	140
<i>Experimental data</i>										
COP										
$T_a = 20^\circ\text{C}(\text{Ex})$	0.75	0.77	0.78	0.79	0.80	0.80	0.80	0.81	0.81	0.81
$T_a = 30^\circ\text{C}(\text{Ex})$	0.67	0.72	0.75	0.77	0.78	0.79	0.80	0.80	0.80	0.81
$T_a = 40^\circ\text{C}(\text{Ex})$	0.33	0.54	0.64	0.69	0.73	0.75	0.77	0.78	0.78	0.79
$T_a = 50^\circ\text{C}(\text{Ex})$	0.00	0.00	0.16	0.45	0.58	0.65	0.69	0.72	0.73	0.74
<i>Simulation data</i>										
COP										
$T_a = 20^\circ\text{C}$	0.79	0.81	0.82	0.83	0.84	0.84	0.85	0.85	0.85	0.85
$T_a = 30^\circ\text{C}$	0.71	0.75	0.78	0.81	0.82	0.83	0.84	0.84	0.85	0.85
$T_a = 40^\circ\text{C}$	0.35	0.57	0.67	0.73	0.77	0.79	0.81	0.82	0.82	0.83
$T_a = 50^\circ\text{C}$	0.00	0.00	0.17	0.47	0.61	0.68	0.72	0.75	0.77	0.78

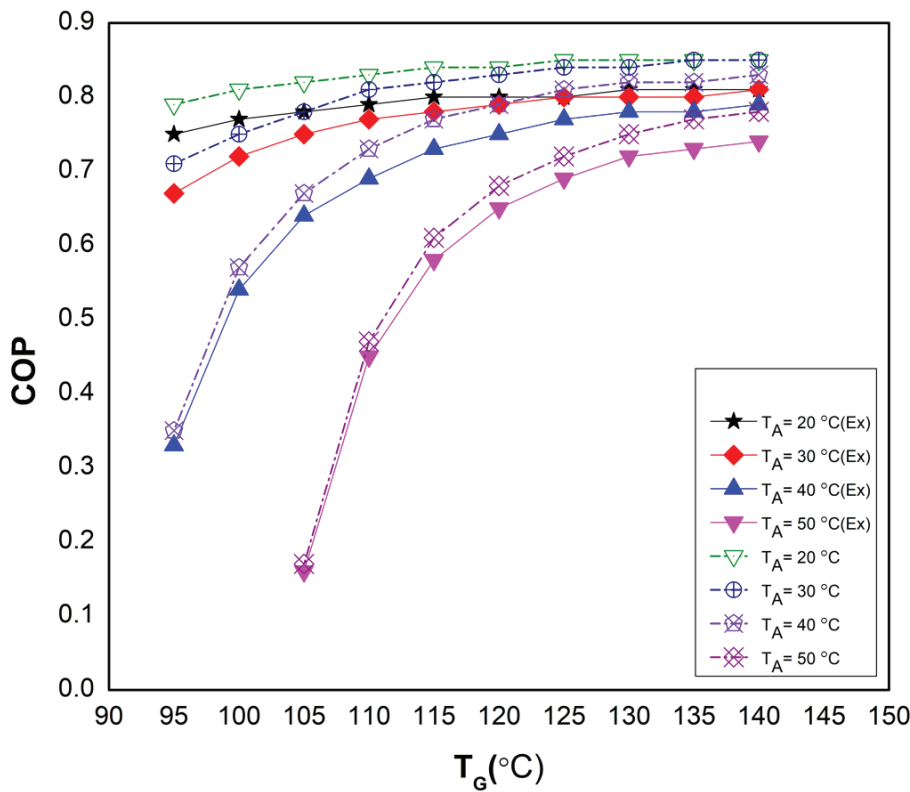


Figure 8. Impact of generator temperature (T_g) on COP ($T_c = 50^\circ\text{C}$, $T_e = 5^\circ\text{C}$, $e_{\text{HX}} = 0.7$).

COP is achieved at low absorber temperature, i.e. 20°C . Similarly, minimum COP is obtained at high absorber temperature, i.e. 50°C . It is due to fact that concentration of the weak solution increases with a rise in generator temperature that also enhance the circulation ratio; hence COP of

absorption system rises. Moreover, simulation and experimental results are in good agreement.

Table 9 shows the experimental and simulation results oncoefficient of performance at different generator temperature with $T_a = 40^\circ\text{C}$, $T_c = 5^\circ\text{C}$, and $e_{\text{HX}} = 0.7$. Figure 9

Table 9. Computed coefficient of performance at different generator temperature ($T_a = 40^\circ\text{C}$, $T_c = 5^\circ\text{C}$, $e_{\text{HX}} = 0.7$)

Generator temperature, T_g ($^\circ\text{C}$)	95	100	105	110	115	120	125	130	135	140
<i>Experimental data</i>										
COP										
$T_c = 20^\circ\text{C}$	0.96	0.96	0.95	0.94	0.92	0.90	0.88	0.86	0.83	0.80
$T_c = 30^\circ\text{C}$	0.88	0.89	0.90	0.90	0.90	0.89	0.88	0.87	0.86	0.85
$T_c = 40^\circ\text{C}$	0.73	0.78	0.80	0.82	0.83	0.84	0.84	0.84	0.84	0.83
$T_c = 50^\circ\text{C}$	0.33	0.54	0.64	0.69	0.73	0.75	0.77	0.78	0.78	0.79
<i>Simulation data</i>										
COP										
$T_c = 20^\circ\text{C}$	1.01	1.00	0.99	0.97	0.95	0.93	0.90	0.87	0.84	0.82
$T_c = 30^\circ\text{C}$	0.94	0.94	0.94	0.94	0.94	0.93	0.92	0.91	0.90	0.93
$T_c = 40^\circ\text{C}$	0.82	0.85	0.86	0.87	0.88	0.88	0.88	0.88	0.88	0.91
$T_c = 50^\circ\text{C}$	0.57	0.67	0.73	0.77	0.79	0.81	0.82	0.82	0.83	0.85

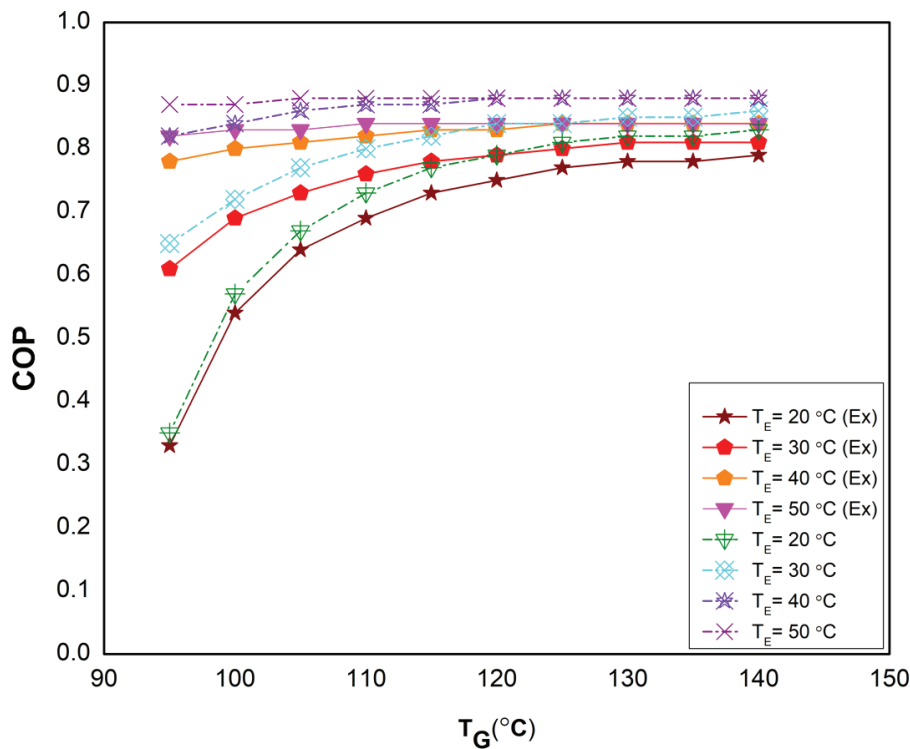


Figure 10. Effect of generator temperature on COP ($T_c = 50^\circ\text{C}$, $T_a = 40^\circ\text{C}$, $e_{HX} = 0.7$).

achieved at high evaporator temperature. Similarly, minimum COP is obtained at low evaporator temperature. This is because of the facts with an increase in generator temperature, the concentration of the strong solution raises which increase the circulation ratio; hence COP of absorption system rises.

Table 11 shows the experimental and simulation results on coefficient of performance at different generator

temperature with $e_{HX} = 0.7$. Figure 11 depicts the variation of condenser, absorber and evaporator temperature with heat exchanger effectiveness of 70%, COP of absorption system increases with increase in generator temperature, at higher values of condenser, absorber and evaporator temperature. Further, at low values of condenser, absorber and evaporator temperature, the COP of the system decreases gradually. This is due to fact that circulation ratio decreases.

Table 11. Computed coefficient of performance at different generator temperature ($e_{HX} = 0.7$)

Generator temperature, T_g ($^\circ\text{C}$)	95	100	105	110	115	120	125	130	135	140
<i>Experimental data</i>										
COP										
$T_c = 20^\circ\text{C}, T_a = 25^\circ\text{C}, T_e = 20^\circ\text{C}$	0.96	0.95	0.95	0.94	0.93	0.91	0.90	0.88	0.86	0.83
$T_c = 30^\circ\text{C}, T_a = 35^\circ\text{C}, T_e = 20^\circ\text{C}$	0.92	0.92	0.92	0.92	0.92	0.91	0.91	0.90	0.89	0.88
$T_c = 40^\circ\text{C}, T_a = 45^\circ\text{C}, T_e = 20^\circ\text{C}$	0.84	0.85	0.87	0.87	0.88	0.88	0.88	0.88	0.87	0.87
$T_c = 50^\circ\text{C}, T_a = 55^\circ\text{C}, T_e = 20^\circ\text{C}$	0.56	0.68	0.74	0.78	0.80	0.82	0.83	0.83	0.83	0.84
<i>Simulation data</i>										
COP										
$T_c = 20^\circ\text{C}, T_a = 25^\circ\text{C}, T_e = 20^\circ\text{C}$	1.01	1.00	1.00	0.99	0.98	0.96	0.95	0.93	0.90	0.87
$T_c = 30^\circ\text{C}, T_a = 35^\circ\text{C}, T_e = 20^\circ\text{C}$	0.97	0.97	0.97	0.97	0.96	0.96	0.95	0.94	0.94	0.93
$T_c = 40^\circ\text{C}, T_a = 45^\circ\text{C}, T_e = 20^\circ\text{C}$	0.88	0.90	0.91	0.92	0.92	0.93	0.93	0.92	0.92	0.92
$T_c = 50^\circ\text{C}, T_a = 55^\circ\text{C}, T_e = 20^\circ\text{C}$	0.59	0.72	0.78	0.82	0.84	0.86	0.87	0.88	0.88	0.88

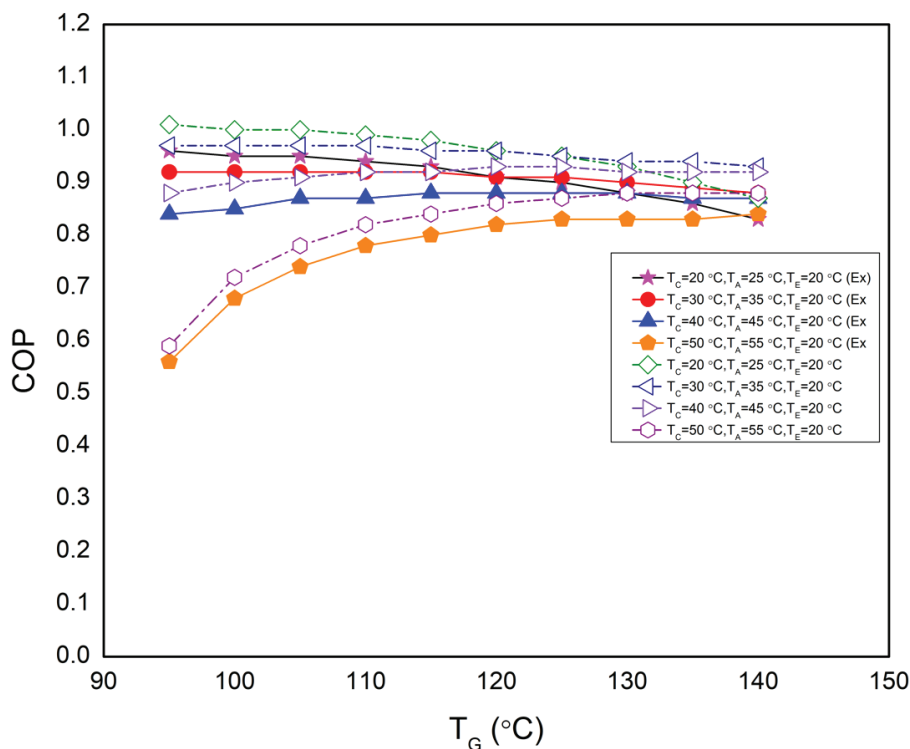


Figure 11. Effect of generator temperature (T_g) on COP ($e_{HX} = 0.7$).

Effect of absorber temperature

In this context, the impact of absorber temperature on heat flow rate in the generator, absorber, condenser, and evaporator, COP of absorption system has been discussed.

Table 12 shows the experimental and simulation results on heat flow rate in generators, absorber, condenser and evaporator at different absorber temperature at $T_g = 110^\circ\text{C}$,

$T_c = 50^\circ\text{C}$, $T_e = 5^\circ\text{C}$, with $e_{SHE} = 0.7$. Figure 12 presents the effect of high absorber temperature (T_a) on the heat flow rate in the generator, absorber, condenser, and evaporator. With increase in absorber temperature, heat flow rate in the absorber and generator increases and its effect on heat flow rate in the condenser, and evaporator is independent, i.e. it remains constant. It is due to fact that with increase of absorber temperature, circulation ratio increases and

Table 12. Computed heat flow rate in generator, absorber, condenser, and evaporator at different absorber temperature ($T_g = 110^\circ\text{C}$, $T_c = 50^\circ\text{C}$, $T_e = 5^\circ\text{C}$, $e_{SHE} = 0.7$)

Absorber temperature, T_a ($^\circ\text{C}$)	20	25	30	35	40	45	50
<i>Experimental data</i>							
Q_a (Ex)	2679.0	2721.8	2756.9	2784.5	2805.4	2820.6	2828.2
Q_c (Ex)	2371.2	2371.2	2371.2	2371.2	2371.2	2371.2	2371.2
Q_e (Ex)	2195.5	2195.5	2195.5	2195.5	2195.5	2195.5	2195.5
Q_g (Ex)	2638.2	2666.7	2722.7	2824.4	3011.5	3409.6	4635.1
<i>Simulation data</i>							
COP							
Q_a	2820.0	2865.0	2902.0	2931.0	2953.0	2969.0	2977.0
Q_c	2496.0	2496.0	2496.0	2496.0	2496.0	2496.0	2496.0
Q_e	2311.0	2311.0	2311.0	2311.0	2311.0	2311.0	2311.0
Q_g	2777.0	2807.0	2866.0	2973.0	3170.0	3589.0	4879.0

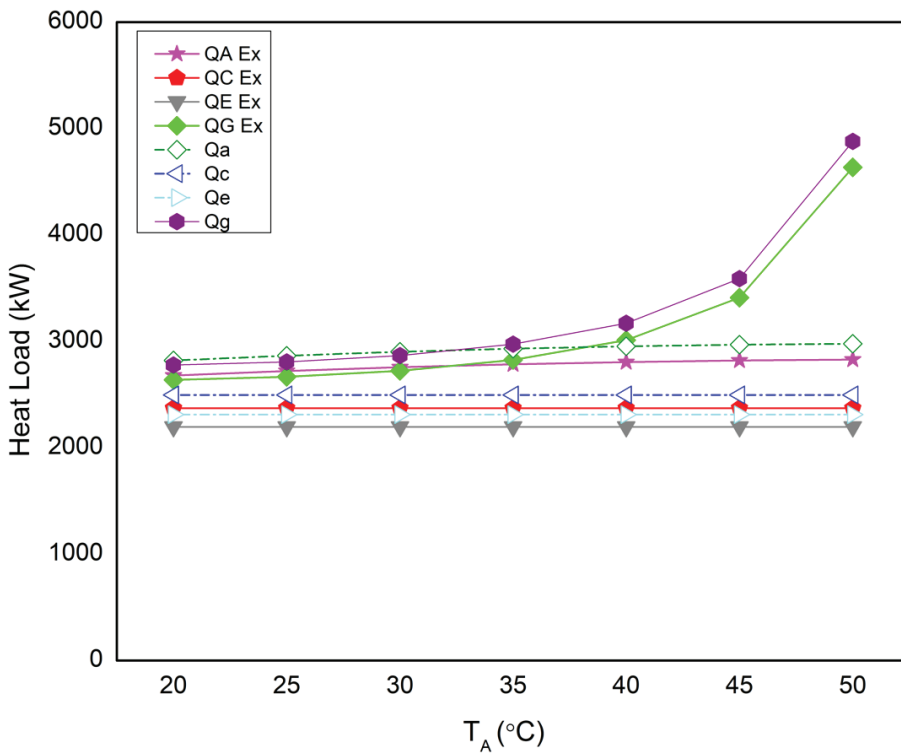


Figure 12. Effect of absorber temperature on heat flow rate in generator, absorber, condenser, and evaporator ($T_g = 110^\circ\text{C}$, $T_c = 50^\circ\text{C}$, $T_e = 5^\circ\text{C}$, $e_{\text{SHE}} = 0.7$).

subsequently increase the heat transfer rate in absorber and generator.

Table 13 shows the experimental and simulation results on the effect of COP in absorber at different condenser temperature with $T_g = 110^\circ\text{C}$, $T_c = 5^\circ\text{C}$, and $e_{\text{SHE}} = 0.7$. Figure 13 depicts that with increase in absorber

temperature, the COP of the absorption system decreases. Further, the values of COP is highest at low temperature-soft condenser and vice-versa. This is because, with a raise in temperature of absorber, the heat exchange rate in generator increases.

Table 13. Computed the effect of COP in absorber at different condenser temperature ($T_g = 110^\circ\text{C}$, $T_c = 5^\circ\text{C}$, $e_{\text{SHE}} = 0.7$)

Absorber temperature, T_a ($^\circ\text{C}$)	20	25	30	35	40	45	50	55	60	65
<i>Experimental data</i>										
COP										
$T_c = 20^\circ\text{C}$ (Ex)	0.93	0.94	0.94	0.94	0.94	0.93	0.92	0.90	0.87	0.84
$T_c = 30^\circ\text{C}$ (Ex)	0.90	0.90	0.91	0.90	0.90	0.89	0.87	0.83	0.79	0.70
$T_c = 40^\circ\text{C}$ (Ex)	0.85	0.85	0.85	0.84	0.82	0.79	0.74	0.66	0.47	
$T_c = 50^\circ\text{C}$ (Ex)	0.79	0.78	0.77	0.74	0.69	0.61	0.45			
<i>Simulation data</i>										
COP										
$T_c = 20^\circ\text{C}$	0.98	0.99	0.99	0.99	0.99	0.98	0.96	0.95	0.92	0.89
$T_c = 30^\circ\text{C}$	0.94	0.95	0.95	0.95	0.94	0.93	0.91	0.88	0.83	0.74
$T_c = 40^\circ\text{C}$	0.89	0.90	0.89	0.88	0.86	0.83	0.78	0.69	0.50	
$T_c = 50^\circ\text{C}$	0.83	0.82	0.81	0.78	0.73	0.64	0.47			

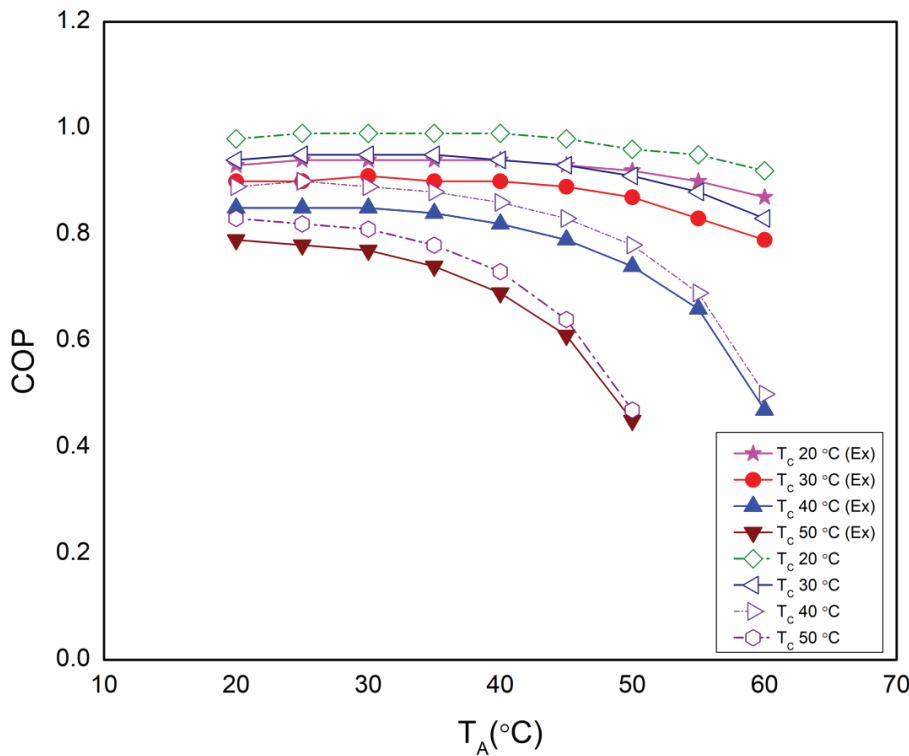


Figure 13. Effect of absorber temperature on COP at different condenser temperature ($T_g = 110^\circ\text{C}$, $T_c = 5^\circ\text{C}$, $e_{\text{SHE}} = 0.7$).

Table 14 shows the experimental and simulation results on COP at different absorber temperature at $T_g = 110^\circ\text{C}$, $T_c = 5^\circ\text{C}$, and $e_{\text{SHE}} = 0.7$. Figure 14 depicts that the COP of the absorption system decreases with increase in absorber temperature. Further, the values of COP is highest at high temperatures of generator and vice-versa. It is due to fact

that concentration of the strong solution increases with an increase in absorber temperature.

Effect of condenser temperature

In this context, the impact of condenser temperature on heat flow rate in the generator, absorber, condenser, and

Table 14. Computed COP at different absorbertemperature ($T_g = 110^\circ\text{C}$, $T_c = 5^\circ\text{C}$, $e_{\text{SHE}} = 0.7$)

Absorber temperature, T_a (°C)	20	25	30	35	40	45	50	55	60	65
<i>Experimental data</i>										
COP										
$T_g = 95^\circ\text{C}(\text{Ex})$	0.75	0.72	0.67	0.57	0.33					
$T_g = 115^\circ\text{C}(\text{Ex})$	0.80	0.79	0.78	0.76	0.73	0.67	0.58	0.38	0.00	0.00
$T_g = 125^\circ\text{C}(\text{Ex})$	0.80	0.80	0.80	0.79	0.77	0.74	0.69	0.61	0.46	0.10
$T_g = 135^\circ\text{C}(\text{Ex})$	0.81	0.81	0.80	0.80	0.78	0.76	0.73	0.69	0.62	0.49
<i>Simulation data</i>										
COP										
$T_g = 95^\circ\text{C}$	0.79	0.76	0.71	0.60	0.35					
$T_g = 115^\circ\text{C}$	0.84	0.83	0.82	0.80	0.77	0.71	0.61	0.40		
$T_g = 125^\circ\text{C}$	0.85	0.85	0.84	0.83	0.81	0.78	0.72	0.64	0.49	
$T_g = 135^\circ\text{C}$	0.85	0.85	0.85	0.84	0.82	0.80	0.77	0.72	0.65	0.52

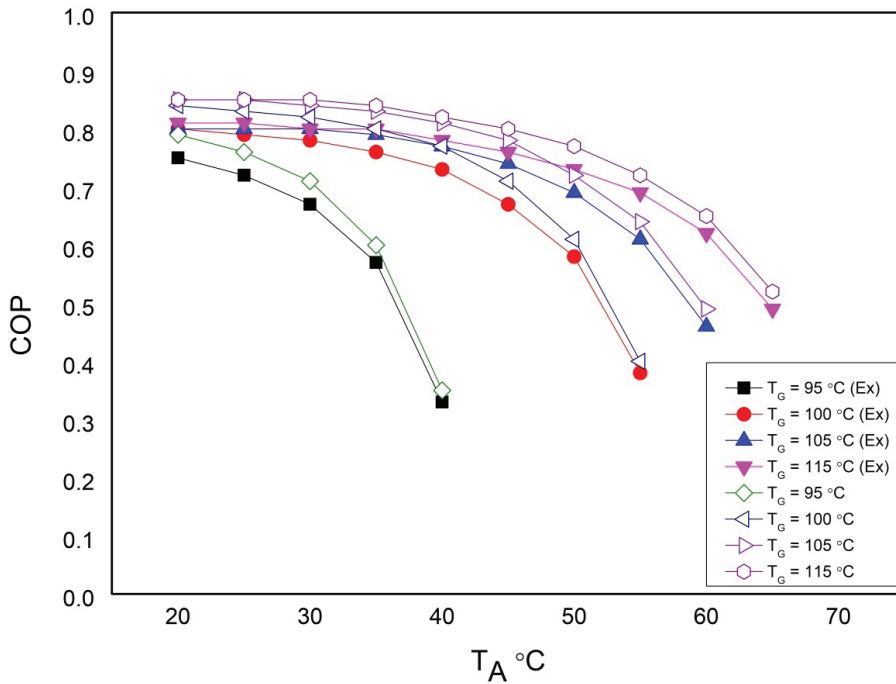


Figure 14. Effect of absorber temperature on COP at different generator temperature ($T_g = 110^\circ\text{C}$, $T_c = 5^\circ\text{C}$, $e_{\text{SHE}} = 0.7$).

evaporator and COP of absorption mechanism have been presented.

Table 15 shows the experimental and simulation results on heat flow rate in generators, absorber, condenser and evaporator at different condenser temperature at $T_g = 110^\circ\text{C}$, $T_a = 40^\circ\text{C}$, $T_c = 5^\circ\text{C}$, and $e_{\text{SHE}} = 0.7$. Figure 15 presents the effect of condenser temperature (T_c) on heat flow rates in the generator, absorber, condenser, and evaporator. Figure 15 depicts that with the increase in condenser

temperature, heat flow rates in absorber, condenser, and evaporator decreases but increases in the generator. This is due to fact that with increase of condenser temperature, circulation ratio increases and consequently increase the heat transfer rate.

Table 16 shows the experimental and simulation results on COP at different evaporator temperature, condenser temperature at $T_g = 110^\circ\text{C}$, $T_a = 40^\circ\text{C}$, and $e_{\text{SHE}} = 0.7$. Figure 16 depicts that with an increase in condenser

Table 15. Computed heat flow rate in generator, absorber, condenser, and evaporator at different condenser temperature at ($T_g = 110^\circ\text{C}$, $T_a = 40^\circ\text{C}$, $T_c = 5^\circ\text{C}$, $e_{\text{SHE}} = 0.7$)

Condenser temperature, T_c ($^\circ\text{C}$)	20	25	30	35	40	45	50	55	60	65
<i>Experimental data</i>										
Q_a (Ex)	2439	2595	2675	2724	2757	2780	2795	2804	2809	2809
Q_c (Ex)	2314	2294	2274	2255	2235	2215	2195	2176	2156	2136
Q_e (Ex)	2537	2518	2498	2478	2457	2437	2417	2397	2377	2356
Q_g (Ex)	2648	2533	2500	2506	2536	2587	2662	2764	2904	3106
<i>Simulation data</i>										
COP										
Q_a	2567	2732	2816	2867	2902	2926	2942	2952	2957	2957
Q_c	2436	2415	2394	2374	2353	2332	2311	2290	2269	2248
Q_e	2671	2650	2629	2608	2586	2565	2544	2523	2502	2480
Q_g	2787	2666	2632	2638	2669	2723	2802	2909	3057	3269

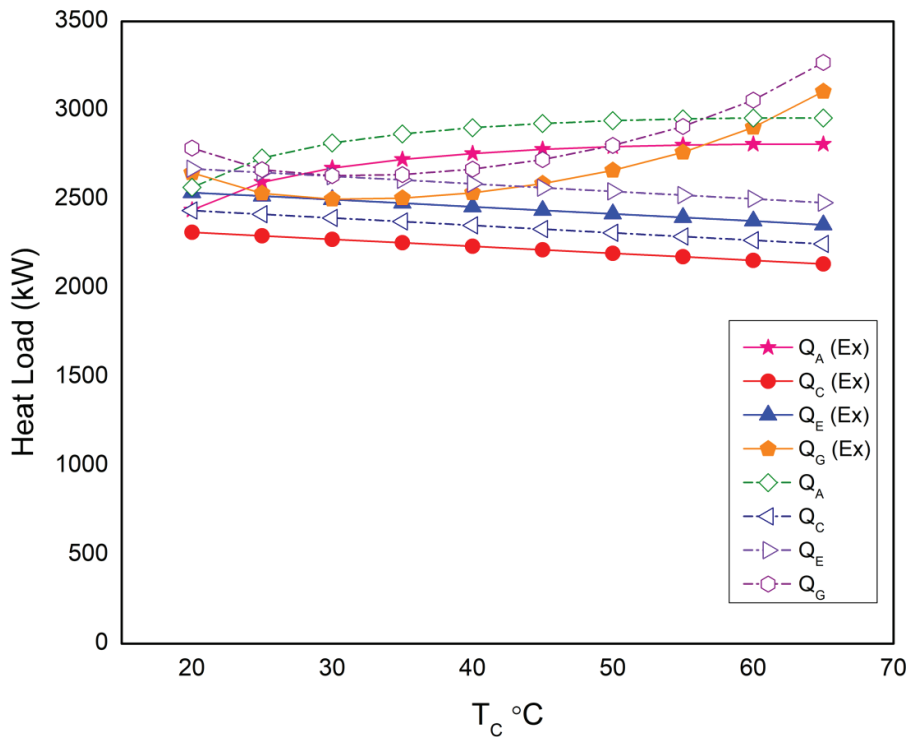


Figure 15. Effect of condenser temperature on heat flow rate in generator, absorber, condenser, and evaporator ($T_g = 110^\circ\text{C}$, $T_a = 40^\circ\text{C}$, $T_e = 5^\circ\text{C}$, $e_{\text{SHE}} = 0.7$).

temperature, the COP of the absorption system decreases at different values of evaporator temperature. Further, the values of COP is highest at high evaporator temperature and vice-versa. This is due to fact that with increase in evaporator temperature, the heat transfer rate in evaporator increases.

Effect of evaporator temperature

In this section, the effect of evaporator temperature on heat flow rate in the generator, absorber, condenser, and evaporator and COP of absorption mechanism have been presented.

Table 16. Computed COP at different evaporator temperature, condenser temperature ($T_g = 110^\circ\text{C}$, $T_a = 40^\circ\text{C}$, $e_{\text{SHE}} = 0.7$)

Condenser temperature, T_c ($^\circ\text{C}$)	20	25	30	35	40	45	50	55	60	65
<i>Experimental data</i>										
COP										
$T_e = 5^\circ\text{C}(\text{Ex})$	0.96	0.93	0.88	0.82	0.73	0.60	0.33			
$T_e = 10^\circ\text{C}(\text{Ex})$	0.98	0.95	0.92	0.87	0.81	0.73	0.61	0.38		
$T_e = 15^\circ\text{C}(\text{Ex})$	0.99	0.97	0.93	0.90	0.85	0.80	0.73	0.62	0.43	
$T_e = 20^\circ\text{C}(\text{Ex})$	0.99	0.97	0.94	0.91	0.87	0.83	0.78	0.72	0.63	0.47
<i>Simulation data</i>										
COP										
$T_e = 5^\circ\text{C}$	1.01	0.98	0.93	0.86	0.77	0.63	0.35			
$T_e = 10^\circ\text{C}$	1.03	1.00	0.96	0.91	0.85	0.77	0.65	0.40		
$T_e = 15^\circ\text{C}$	1.04	1.02	0.98	0.94	0.90	0.84	0.77	0.66	0.45	
$T_e = 20^\circ\text{C}$	1.05	1.02	0.99	0.96	0.92	0.87	0.82	0.76	0.67	0.49

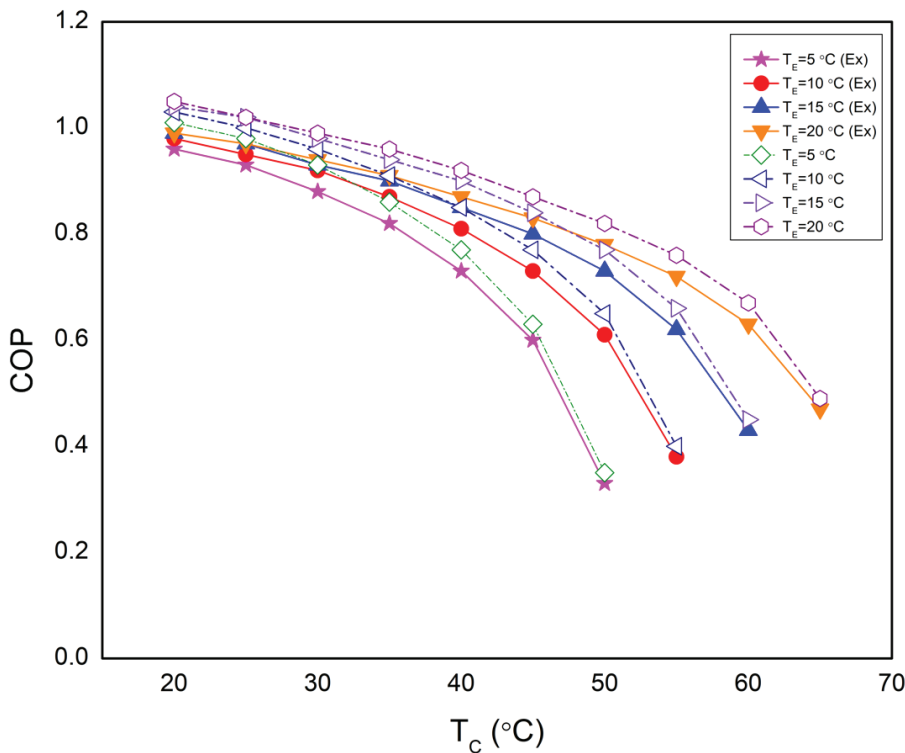


Figure 16. Impact of condenser temperature on COP at variant evaporator temperature ($T_g = 110^\circ\text{C}$, $T_a = 40^\circ\text{C}$, $e_{\text{SHE}} = 0.7$).

Table 17 shows the experimental and simulation results on COP at different evaporator temperature at $T_g = 110^\circ\text{C}$, $T_a = 40^\circ\text{C}$, $T_c = 50^\circ\text{C}$, and $e_{\text{SHE}} = 0.7$. Figure 17 depicts that the COP of the absorption system increases with increase in evaporator temperature at different values of generator temperature. This is due to fact that at low pressure,

the enthalpy at evaporator exit increases. Further, with an increment in generator temperature, the concentration of the weak solution increases too which increases the COP of the absorption system. In other words, refrigeration capacity increases and heat transfer in HTG decreases. Thus, COP of system increases at different generator temperature.

Table 17. Computed COP at different evaporator temperature ($T_g = 110^\circ\text{C}$, $T_a = 40^\circ\text{C}$, $T_c = 50^\circ\text{C}$, $e_{\text{SHE}} = 0.7$)

Evaporator temperature, T_e ($^\circ\text{C}$)	6	8	10	12	14	16	18	20	22	24
<i>Experimental data</i>										
COP										
$T_g = 95^\circ\text{C}$	0.42	0.53	0.61	0.67	0.71	0.74	0.76	0.78	0.80	0.81
$T_g = 115^\circ\text{C}$	0.74	0.76	0.78	0.79	0.81	0.82	0.82	0.83	0.83	0.84
$T_g = 125^\circ\text{C}$	0.78	0.79	0.80	0.81	0.82	0.83	0.83	0.84	0.84	0.84
$T_g = 135^\circ\text{C}$	0.79	0.80	0.81	0.82	0.83	0.83	0.84	0.84	0.84	0.84
<i>Simulation data</i>										
COP										
$T_g = 95^\circ\text{C}$	0.44	0.56	0.65	0.70	0.75	0.78	0.81	0.82	0.84	0.85
$T_g = 115^\circ\text{C}$	0.78	0.80	0.82	0.84	0.85	0.86	0.87	0.87	0.88	0.88
$T_g = 125^\circ\text{C}$	0.82	0.83	0.84	0.86	0.86	0.87	0.88	0.88	0.88	0.88
$T_g = 135^\circ\text{C}$	0.83	0.84	0.85	0.86	0.87	0.88	0.88	0.88	0.88	0.89

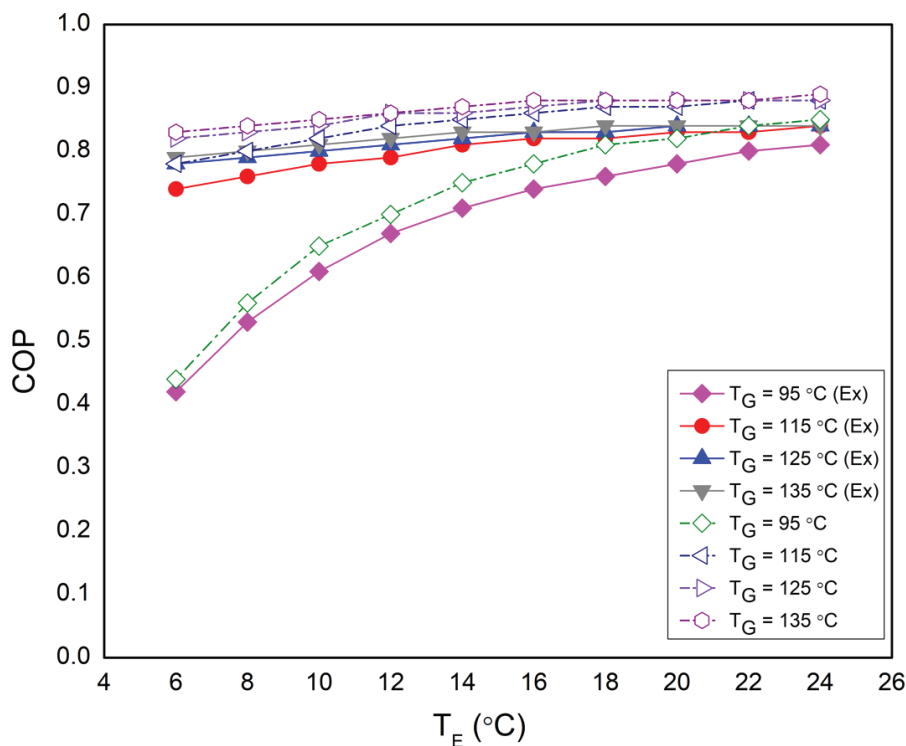


Figure 17. Impact of evaporator temperature on COP of absorption system ($T_g = 110^\circ\text{C}$, $T_a = 40^\circ\text{C}$, $T_c = 50^\circ\text{C}$, $e_{\text{SHE}} = 0.7$).

CONCLUSION

The experimental and numerical research on a LiBr-water vapor absorption system has been conducted. The experimental values of COP and circulation ratio of the vapor absorption system have been compared with the values predicted using EES. The effect of operating variables on LiBr-Water absorption system has been done over a broad range of operating conditions for the feasibility assessment in the dairy industry. The conclusions drawn from the analysis have been summarized as:

- A simulation model has been developed, and the results have been compared with the experimental outcome. The results of both the simulation and the experiments have been observed to be in good agreement of 5.3%.
- The COP of the system increased with raise in the generator temperature at different temperatures of absorber and evaporator. However, the COP decreased by varying the temperature of the condenser due to a decrease in circulation ratio. Further, under the simultaneous variations in temperature of absorber, condenser and evaporator, the COP of the system decreased.
- The rate of heat exchanger in absorber and condenser has been observed to be increased with a rise in generator temperature. Although, the rate of heat exchange in the generator decreased gradually as the circulation ratio tend to fall. Moreover, the impact of the rise of generator temperature on heat transfer in evaporator

remains constant. It is since the increase in generator temperature cause the circulation ratio to decrease.

- The heat flow rates in the generator and absorber increased with the increase in absorber temperature while remained constant in the condenser and evaporator due to the rise in circulation proportion.
- The heat flow rates in absorber, condenser and evaporator decreased with the increase in condenser temperature while increased in the generator.
- It has been observed that with the increase in evaporator temperature the heat transfer rate in the absorber and the generator decreased while increased in the evaporator. Moreover, heat transfer in the condenser remained constant. The main reason for the drop of heat transfer in the absorber was that the circulation proportion tends to decline, and the concentration of less stable solution leaving from the generator increased. The decline of heat transfer in the generator was because of the gradual drop of enthalpy of refrigerant entering the condenser.
- According to study conducted by Yildrem and Genc [11] the heat required in dairy industry for process heat application is 2375kW. In this research work heat rejected from the condenser of the experimental facility has been observed to be in same range approx. (2100 – 2400 kW) that is quite sufficient to fulfil the requirement of a dairy industry.

NOMENCLATURE

Symbols and abbreviations

COP	Coefficient of performance
CR	Circulation ratio
EES	Engineering equation solver
LiBr	Lithium bromide
\dot{m}	Mass flow rate (kg/s)
\dot{m}_r	Mass flow rate of refrigerant (kg/s)
P	Pressure (kPa)
Q _e	Refrigerating effect (kW)
Q _G	Heat input of generator (kW)
T	Temperature (°C)
T _a	Absorber temperature (°C)
T _b	Boundary temperature (K)
T _c	Condenser temperature (°C)
T _e	Evaporator temperature (°C)
T _g	Generator temperature (°C)
X	Concentration of Lithium bromide in solution (%)

Subscripts

a, Abs	Absorber
c	Condenser
D	Destruction
e	Evaporator
g	Generator
Ex.	Expansion
i	Represents, corresponding state points
o	Outlet condition
p	Pump
r	Refrigerant
RTV	Expansion valve
S	Strong
SHE	Solution heat exchanger
STV	Solution throttle valve
W	Weak

ACKNOWLEDGEMENT

The writers oblige the recognition of the experimental test facility given through the National Institute of Solar Energy (NISE), Gurugram, India.

AUTHORSHIP CONTRIBUTIONS

Authors equally contributed to this work.

DATA AVAILABILITY STATEMENT

The authors confirm that the data that supports the findings of this study are available within the article. Raw data that support the finding of this study are available from the corresponding author, upon reasonable request.

CONFLICT OF INTEREST

The author declared no potential conflicts of interest with respect to the research, authorship, and/or publication of this article.

ETHICS

There are no ethical issues with the publication of this manuscript.

REFERENCES

- [1] Desai DD, Raol JB, Patel S, Chauhan I. Application of Solar energy for sustainable Dairy Development. *Eur J Sustain Dev* 2013;2:131–140. [CrossRef]
- [2] Yadav R, Jadhav V, Chougule G. Exploring the scope of renewable energy technologies in dairy sector. *Int J Eng Sci Res Technol* 2016;5:439–450.
- [3] Abu-Khader M. Recent progress in CO₂ capture/sequestration: A review. *Energy Sources Part A* 2006;28:14:1261–1279. [CrossRef]
- [4] Şencan Şahin A, Kovacı T, Dikmen E. A GEP model for energy and exergy analysis of LiCl-H₂O absorption cooling systems. *Energy Sources Part A* 2019;43:4. [CrossRef]
- [5] Sharma A, Kaushal R. Experimental investigation of a novel multi-channel flat plate liquid desiccant dehumidification system. *Energy Sources, Part A* 2021;1–19. [CrossRef]
- [6] Uçkan İ, Yousif AA. Investigation of the effect of various solar collector types on a solar absorption cooling system. *Energy Sources Part A* 2020;7:875–892. [CrossRef]
- [7] Bhatewara A, Stephan D. 746c898f321af3d1a1d-0b6714acb701ddf80b016 @ www.process-worldwide.com, 2013. Available at: <https://www.process-worldwide.com/solar-energy-for-india-dairy-industry-a-419153/> Accessed on May 15, 2023.
- [8] Guiney W. 69cbbb4475f94c9da4ed0ed494891d1918bc9388@www.thomasnet.com. 2008, Available at: <https://www.thomasnet.com/insights/pasteurization-and-refrigeration-for-milk-and-dairy-products/> Accessed on May 15, 2023.
- [9] Zhang C, Campana P, Yang J, Zhang J, Yan J. Can solar energy be an alternative choice of milk production in dairy farms? -A case study of integrated PVWP system with alfalfa and milk production in dairy farms in China. *Energy Proced* 2017;105:3953–3959. [CrossRef]
- [10] Panchal H, Patel R, Chaudhary S, Patel DK, Sathyamurthy R, Arunkumar T. Solar energy utilisation for milk pasteurisation: A comprehensive review. *Renew Sustain Energy Rev* 2017;92:1–8. [CrossRef]
- [11] Yildirim N, Genc S. Thermodynamic analysis of a milk pasteurization process assisted by geothermal energy. *Energy* 2015;90:987–996. [CrossRef]
- [12] Cocco D, Tola V, Petrollese M. Application of concentrating solar technologies in the dairy sector for the combined production of heat and power. *Energy Proced* 2016;101:1159–1166. [CrossRef]

- [13] Bhatewara A. Application of solar thermal in dairy industry. *Int Renew Energy Agency* 2017;2:86291.
- [14] Sandey KK, Agrawal AK, Nikam P. Solar water heating- potential use in dairy industry. *Int J Eng Res Technol* 2015;3:3–4.
- [15] Anderson TN, Duke M. Solar energy use for energy savings in dairy processing plants. *IPENZ Eng TreNz* 2008;1:1–9.
- [16] Modi A, Prajapat R. Pasteurization process energy optimization for a milk dairy plant by energy audit approach. *Int J Sci Technol Res* 2014;3:181–188.
- [17] Ketfi O, Merzouk M, Merzouk NK, El Metenani S. Performance of a single effect solar absorption cooling system (LiBr-H₂O). *Energy Proced* 2015;74:130–138. [\[CrossRef\]](#)
- [18] Manu S, Chandrashekar TK. A simulation study on performance evaluation of single-stage LiBr-H₂O vapor absorption heat pump for chip cooling. *Int J Sustain Built Environ* 2016;5:370–386. [\[CrossRef\]](#)
- [19] Lamine CM, Said Z. Energy analysis of single effect absorption chiller (LiBr/H₂O) in an industrial manufacturing of detergent. *Energy Proced* 2014;50:105–112. [\[CrossRef\]](#)
- [20] Pandya B, Patel J, Mudgal A. Thermodynamic evaluation of generator temperature in liBr-water absorption system for optimal performance. *Energy Proced* 2016;109:270–278. [\[CrossRef\]](#)
- [21] Patel HA, Patel LN, Jani D, Christian A. Energetic analysis of single stage lithium bromide water absorption refrigeration system. *Procedia Technol* 2016;23:488–495. [\[CrossRef\]](#)
- [22] Uçkan I, Yousif A. Simulation of a solar absorption cooling system in Dohuk city of the Northern Iraq. *Energy Sources Part A* 2020;42:1716–1732. [\[CrossRef\]](#)
- [23] Iyer GV, Nagar V, Road M, Mastorakis NE, Theologou AI. Energy conservation measures in dairy industries. *Proceedings of the 4th WSEAS International Conference on Fluid Mechanics and Aerodynamics, Elounda, Greece, August 21-23, 2006*, p. 435–444.
- [24] Singh M, Kele VD, Chavan B, Ranvir S, Dhotre AV. A review on solar water heating systems and its use in dairy industry. *Int J Curr Microbiol Appl Sci* 1975;8:1975–1986. [\[CrossRef\]](#)
- [25] Zhu L, Gu J. Second law-based thermodynamic analysis of ammonia/sodium thiocyanate absorption system. *Renew Energy* 2010;35:1940–1946. [\[CrossRef\]](#)
- [26] Singh DV, Verma TN. Comment on "first and second law analysis of ammonia/salt absorption refrigeration systems by L. Garousi Farshi et al. [*Int. J. refrigeration* 40 (2014) 111-121]". *Int J Refrig* 2020;109:208–209. [\[CrossRef\]](#)
- [27] Singh DV, Verma TN. Energy analysis of water-lithium chloride (LiCl-H₂O) operated absorption refrigeration system using ann approach. *Int J Eng Adv Technol* 2019;8:225–232.
- [28] Balas VE. *Advances in Intelligent Systems and Computing 634 Soft Computing Applications. Proceedings of the 7th International Workshop Soft Computing Applications. Vol. 2, (SOFA 2016).* [\[CrossRef\]](#)
- [29] Mebarek-Oudina F. Numerical modeling of the hydrodynamic stability in vertical annulus with heat source of different lengths. *Eng Sci Technol Int J* 2017;20:1324–1333. [\[CrossRef\]](#)
- [30] Shaaban AM, Antar MA, Khalifa AE, El-Shaarawi MA. Analysis of integrated H₂O-LiBr absorption cooling and single-effect evaporation desalination system. *Arab J Sci Eng* 2020;45:5273–5284. [\[CrossRef\]](#)
- [31] Modi B, Mudgal A, Patel B. Energy and Exergy Investigation of Small Capacity Single Effect Lithium Bromide Absorption Refrigeration System. *Energy Proced* 2017;109:203–210. [\[CrossRef\]](#)
- [32] Kaushik SC, Arora A. Energy and exergy analysis of single effect and series flow double effect water-lithium bromide absorption refrigeration systems. *Int J Refrig* 2009;32:1247–1258. [\[CrossRef\]](#)
- [33] Moffat RJ. Describing the uncertainties in experimental results. *Exp Therm Fluid Sci* 1988;1:3–17. [\[CrossRef\]](#)